Article:
Li, Q, Li, X, Yang, K et al. (4 more authors) (2021) The long-term failure mechanisms of alkali-activated slag mortar exposed to wet-dry cycles of sodium sulphate. Cement and Concrete Composites, 116. 103893. ISSN 0958-9465

https://doi.org/10.1016/j.cemconcomp.2020.103893

The Long-Term Failure Mechanisms of Alkali-Activated Slag Mortar Exposed to Wet-dry Cycles of Sodium Sulphate

Qing Li[a,b], Xinyuan Li[b], Kai Yang[b,c*], Xiaohong Zhu[b,c*], Juan Pablo Gevaudan[c,d], Changhui Yang[b], Muhammed Basheer[c]

a: College of Civil and Architectural Engineering, Guilin University of Technology, China, 541004
b: College of Materials Science and Engineering, Chongqing University, China, 400045
c: School of Civil Engineering, University of Leeds, Leeds, UK, LS2 9JT
d: Architectural Engineering Department, Pennsylvania State University, State College, USA, 16802

Abstract: This study investigates the long-term (570 days) performance of alkali-activated slag (AAS) mortar materials exposed to combined wet-dry cycles and sodium sulphate solutions (i.e. 5 wt.% and 10 wt.%). Physical and mechanical characteristics of AAS mortars (i.e., visual appearance, compressive/flexural strength, mass change, capillary porosity, water sorptivity) as well as mineralogical and chemical parameters were determined via XRD, FTIR, DSC and BSE. Findings were compared to Portland cement (PC) and high sulphate resistant (HSR) samples. Results indicate that AAS mortars perform better than PC and HSR samples with minimal changes to compressive strength at 570 days (1.7 % increasement). The main failure mode for AAS mortar was external spalling, which could be due to the crystallisation/dissolving pressure of sodium sulphate. Moreover, the results indicate key differences in the deterioration mechanism of AAS. Unreacted slag, exposed during sodium sulphate attack under wet-dry cycles, can continue to react in sodium sulphate to form silicon-rich gels. The formation of highly siliceous gel regions has beneficial impacts, such as the increase in flexural strength. While no calcium sulphate phases were detected via XRD and FTIR after 570 days of exposure, it is evident that the molecular changes to the microstructure reveal depolymerisation and enhanced formation of Si-O phases after long-term sodium sulphate exposure. These results are important to understand the long-term degradation mechanisms of AAS materials exposed to sodium sulphate under wet-dry cycles.

Keywords: alkali-activated slag material, deterioration, crystallisation and dissolving stress, sulphate attack, wetting and drying cycles

1. Introduction

Ground granulated blast-furnace slag (GGBFS) is an industry by-product of blast furnace ironmaking [1]. Once activated by alkali metal compound activators such as sodium hydroxide and/or sodium metasilicate, GGBFS will dissociate and re-associate to form C(N)-A-S-H and other reaction products, which is generally named as alkali-activated slag (AAS) cement [2-4]. AAS cement has many advantages including high strength and excellent resistance against acid [5], alkaline and chemical attacks [6], lower CO_2 emission and energy consumption in comparing to ordinary Portland cement (PC) [7]. Despite their favourable performance, AAS material also faces many challenges before its application, such as extensive shrinkage and cracking [8, 9], high risk of efflorescence [10], high susceptibility to alkali-silica reaction [11], and unclear performance in chloride-bearing environments [12]. Perhaps one of the most significant conundrums impeding the implementation of AAS concrete is their long-term durability. The ability to resist sodium sulphate attack is a key indicator to evaluate durability of cement-based materials. AAS cement exhibits strong resistance against sulphate chemical attack, which has been reported in numerous studies. This is due to the absence of calcium hydroxide and stably bonded aluminium phases [13-16], meaning that the typical sulphate erosion products (such as gypsm and ettringite) are hardly formed in AAS cement [17, 18]. Furthermore, the pH pore solution of AAS is higher than that of PC [19], where the formation of erosion products in AAS, if any, is also not stable.

However, AAS materials will not only suffer from chemical attack of sulphate in service, but also suffer physical crystallisation damage of sulphates when exposed to alternating wet-dry environments (e.g., wave-splashing area and tidal zone). In the research field of PC, more and more attention has been paid to sulphate

crystallisation failure. On base of the achievements have been made in PC materials, the performance decay is increased, when PC is partially replaced by GGBFS as a supplementary cementitious material. Ganjian and Pouya [20] studied the performance of cement concrete specimens with 50% GGBFS in a simulated tide exposure condition and the results showed that the peeling of GGBFS-supplemented concrete was kinetically faster than that of the PC control. Gruyaert et al. [21] also found that sodium sulphate damage became more serious than the control group, when the dosage of GGBFS increased (i.e., 50%, 70%, 85%). Adding to the severity of this mode of degradation, the water absorption rate of AAS is two to three times higher than that of PC [22, 23], which exacerbates the sodium sulphate crystal dissolution rate and increases diffusion stress. Moreover, the ionic concentration of pore liquid in AAS is higher, especially alkali metal ions, which are usually ten times higher than that of PC [24]. This means that the ions in the pores of AAS are more likely to reach supersaturation state, and then generate crystallisation pressure. What is more, the pore size of AAS materials is mainly distributed between 1~20 nm, while pore size in PC is between 10~100nm [25, 26]. The pore size of AAS is smaller than that of PC, which means that crystallisation pressure is higher. It is not difficult to see from the above that the AAS material is faced with serious risk of physical crystallisation failure of sodium sulphate. To the authors knowledge, little is understood about the behaviour of AAS concrete to wet-dry cycles in combination with sodium sulphate attack. This results in that engineers cannot accurately evaluate the sulphate resistance of AAS.

To bridge the gap in knowledge, this study investigates the long-term degradation behaviours (570 days) of AAS mortar under wet-dry cycles and sodium sulphate exposure (0 wt.%, 5 wt.%, and 10 wt.%). Physical deterioration of AAS mortar was characterised by visual inspection, mechanical properties, mass change, porosity and water sorptivity. Analysis of chemical and physical microstructural aspects were examined with X-ray diffraction (XRD), Fourier-transform infrared spectroscopy (FTIR), differential scanning calorimetry (DSC) and backscattered electron (BSE). Behaviours of AAS samples were also compared with both PC and high sulphate resistant (HSR) cement material specimens to illustrate the differences in performance among common binders.

2. Experimental programme

2.1 Raw materials

GGBFS provided by Chongqing Iron and Steel Company was grounded in a ball mill for 30 minutes, and then grounded in a vibration mill for another 20 minutes. After this, the specific area and density of GGBFS were measured and its Blaine fineness and density were 505 m^2/kg and 2.95 g/cm^3. PC (CEM I: Blaine fineness: 350 m^2/kg, density: 3.15 g/cm^3) and HSR cement (Blaine fineness: 380 m^2/kg, density: 3.2 g/cm^3) complying with the Chinese National Standard GB175-2007 [24] and Chinese National Standard GB748-2005 respectively, were used to prepare PC and HSR samples. It should be pointed out that, in this study, the slag was prepared for using in a fast-repairing project and the slag is finer than PC and HSR. Even though, the composition of reaction products in AAS would not change significantly, and thus the deterioration mechanism of AAS subjected sulphate attack should be relevant consistent. We highlighted that PC and HSR is used to illustrate differences in the deterioration process with AAS cement.

Table 1 summarises the chemical compositions of the GGBFS, PC and HSR cement used in this study. The content of siliceous components (SiO_2, 34.52%) in GGBFS in higher than that of PC and HSR, as well as the content of aluminous components (Al_2O_3, 13.65%). The content of aluminous components (Al_2O_3, 0.62%) and ferrous components (Fe_2O_3, 0.62%) is quite low in HSR, which is favourable to resistant against sodium sulphate attack.

Siliceous sand (instead of calcareous sand) with a fineness modulus of 2.6 was selected to minimise the influence of limestone powder in sodium sulphate environments. Because the limestone is not always inert in the binder materials, especially subjected to strongly alkaline and/or sulphate environment, which have been proved by studies [28-30]. The limestone powder might provide the calcium to form gypsum, making the

degradation of mortars more complex. This study intends to focus on analysing degradation mechanisms of AAS mortars under wet-dry cycles with sodium sulphate and hence, calcareous sand is not selected.

The AAS binders were prepared at the activator (Na_2O) concentration of 5 wt.% of GGBFS. The alkaline activator was a sodium silicate solution with a silica modulus (Ms, SiO_2/Na_2O molar ratio) of 1.5. It was prepared by mixing the NaOH solution and commercial sodium silicate (Ms=2.2) in a pre-calculated ratio. In order to avoid influences of dissolution heat on experimental results, the alkaline solution was cooled at a constant temperature of 20 ± 1 ^oC for two hours prior to mixing. The sodium sulphate solutions were prepared by mixing the sodium sulphate pellets with hot water (about 30 ^oC) according the pre-calculated ratio, and then cooled to 20 ^oC before the mortar specimens were put in.

2.2 Sample preparation and wet-dry regime

AAS, HSR, and PC samples were produced in accordance to the proportions presented in **Table 2**. The sand and binder were mixed in a stirring vessel at low speed for 30s, and then the weighed solution (water and/or activator) was added during the second 30s. A high-speed mixing was applied after 60s followed by a stop of 30s to scrap the mortar off the blade and walls into the pot. The mortar was then stirred for another 30s before casting into $40 \times 40 \times 160$ mm^3 moulds. The mixing procedures were applied according to the Chinese standard GB 17671-1999 [31]. After casting, specimens were compacted on a vibration table until no air bubbles appeared on the surface and then, covered with thick polythene sheets to prevent moisture loss. All specimens were de-moulded after one day and moved into a standard curing room (20 ± 2 ^oC, RH > 95%) for 28 days.

After 28 days of curing, AAS mortar specimens were placed in tanks of water and sodium sulphate solutions with concentrations of 5 wt.% (N5) and 10 wt.% (N10). PC and HSR samples were utilised as the reference and placed in sodium sulphate solutions with concentrations of 5 wt.%. The volume ratio of specimens and sodium sulphate solutions is 1:20 and solutions were renewed every month. The wet-dry regime consisted of immersion for 7 days at 20 ^oC followed by drying for 7 days at 40 ^oC. Thus, in this study sample nomenclature of AAS-Water refers to an AAS mortar samples that has been exposed to water, while AAS-N5 and AAS-N10 refer to AAS mortar samples exposed to 5 wt.% and 10 wt.% sodium sulphate solutions, respectively. Lastly, HSR-N5 and PC-N5 refers to HSR and PC samples exposed to 5 wt.% sodium sulphate solutions. It should be highlighted that effect of leaching under the action of wet-dry cycles can't be avoidable, even this, it would be possible to analyse the changes of AAS properties is caused by leaching and/or sulphate attack through careful comparing between AAS samples exposed to water and sodium sulphate.

2.3 Test methods

2.3.1 Visual appearance of mortar samples

In order to observe visual changes of mortar specimens after sodium sulphate attack during wet-dry cycles, the mortar specimens were cleaned using hairbrush, and the appearance of specimens were recorded by optical camera at 30, 60, 120, 180, 270, 360, 450, and 570 days; where 0 days refers to samples after 28 days of curing.

2.3.2 Compressive/flexural strength

To test the mechanical properties of mortar specimens, which is concerned by the engineering community, compressive strength and flexural strength of samples were determined according to the Chinese National Standard GB/T17671-1999 [31] at the exposure duration of 30, 60, 120, 180, 270, 360, 450, and 570 days. All the results of flexural strength reported are the average value of three specimens, and the results of compressive strength are the average value of six specimens.

2.3.3 Mass change

Mass change is one essential index to evaluate the resistance of mortars to sulphate under wet-dry cycles. The mass variation of damaged specimens was tested by recording the weight of each specimen at each exposure duration (30, 60, 120, 180, 270, 360, 450, and 570 days) and comparing it to the initial weight. The percent

change was calculated using **equation 1**, where M_C is the increase in weight of samples (%); m_0 is the weight of specimen at the initial attack age (g); m_t is the weight of specimens at each testing age (g).

$$M_C = \frac{m_t - m_0}{m_0} \quad (1)$$

2.3.4 Capillary porosity

The capillary porosity can reflect the change of pore structure of mortar specimens in a certain extent. It was assessed by measuring accessible porosity according to ASTM C642 [32]. At the specific ages, the mortar samples were saturated by immersing into a water tank at 20 °C (boiling was not used to avoid potential changes in samples) and the mass of the surface dried specimen was measured after immersion for 72 hours. The surface moisture was removed by a towel, and the mass was determined, m_{imm}. Then, the specimen was suspended by a wire and its apparent mass in water was determined, m_{sus}. After this, the mortar samples were dried in an oven at a temperature of 40 °C until constant weight was reached and were placed in a desiccator at room temperature, so the dry mass, m_{dry}, was measured. The capillary porosity can be determined by using **equation 2**, where ϕ_C denotes the capillary porosity (%); m_{imm} denotes the mass of the surface-dried specimen (g); m_{dry} denotes the mass of specimen after drying at 40 °C (g); and m_{sus} denotes the mass of specimen suspended in water (g).

$$\phi_C = \frac{(m_{imm} - m_{dry})}{m_{imm} - m_{sus}} \quad (2)$$

2.3.5 Water sorptivity test

Water sorptivity is a parameter to control sulphate ions transport in mortars. No drying methods have been developed for AAS to date and the effect of different drying techniques on the microstructure of AAS samples is not well studied. Therefore, before carrying out the experiments reported in this study, relevant standards and recommendations for sorptivity measurements were cross compared, including ASTM: C1585 [33], RILEM: TC-116 [34], BS-EN:13057 [35] and BS: 1811-122 [36]. It should be highlighted is that the drying temperature generally varies from 40 °C to 80 °C to remove free moisture in the sample and after drying for a specific duration, the samples are placed in an air-tight container for 10 days to 15 days to redistribute the moisture. Considering these standards for testing, in this study, the sorptivity of mortar samples was determined according to the procedures described in [22]. Hence, test specimens were dried in an oven at 40 °C, RH≈35% for 7 days before carrying out sorptivity tests. After drying, the specimens were kept in a desiccator for 1 day to cool down to the room temperature. In the sorptivity test, besides the bottom surface that is in contact with water, all other surfaces were sealed to avoid water loss or gain from the environment. Water was absorbed through the bottom surface and the mass increase of the specimens was measured every minute over a period of 25 min. To calculate the value of sorptivity, the data points were fitted using **Equation 3:**

$$i = a + St^{0.5} \quad (3)$$

where i is the volume of water absorbed per unit area (mm^3/mm^2); S is a material constant called the sorptivity ($mm/min^{0.5}$); a is a constant (mm) and t is the time elapsed (min). It should be highlighted is that the data used for calculating water sorptivity are results before the absorption reaches equilibrium to avoid the influence of moisture diffusion.

2.3.6 X-ray diffraction (XRD)

XRD was used to analysis the product composition of mortars. To prepare the samples for XRD measurements, the mortar specimens were dried in a blast air oven at 40 °C for 3 days and then, they were crushed and ground into powders (particle size less than 75 μm). A PANalytical's XPert Pro X-ray diffractometer with nickel-filtered Cu Kαl radiation 1.5405 Å, 40 kV voltage and 40 mA current with scanning speed of 2°/min was used

to identify crystalline phases presented in the samples. The scanned range was between 5° to 70° (2θ).

2.3.7 Fourier transform infrared spectroscopy (FTIR)

In order to determine the chemical groups in reaction products, fourier transform infrared analysis was carried out using the KBr pellet method (1 mg sample per 100 mg KBr). The instrument (5DXC from America Nicolet) with 32 scans per sample collected from 4,000 to 400 cm^{-1} at 4 cm^{-1} resolution was set for FTIR measurements. The powder samples were prepared by the method described in 2.3.6.

2.3.8 Thermogravimetric analysis (DSC)

The evolution of product structure was invested by thermogravimetric analysis. The DSC was tested using STA250 (Netzsch, Germany). Mortar samples were crushed, transferred immediately to an alumina crucible and were held under isothermal conditions for 30 min at 20 ºC to equilibrate in a nitrogen environment. The temperature was raised from the room temperature (20 ± 1 ºC) to 1000 ºC with a rate of 10 ºC/min and the weight change was monitored continuously.

2.3.9 Back scattered electron imaging (BSE)

Back scattered electron imaging analysis was employed to assess microstructure features of AAS and PC. At the testing age, a cube about 10 mm was cut from the middle part of mortar using the precision cutting machine (Brand: YJ-425CNC, Made in Wenzhou China). The specimens were then vacuum dried for 3 days at a constant temperature of 40 (±1) ºC, after which specimens were coated with gold using a sputtering device. The TESCAN VEGA 3 LMH fitted with a tungsten filament emission source was used to capture the images of two depth area (around 0.5mm and 3mm, see **Figure 1**). The depth of observation surface could be obtained using the standard ruler of electron microscope. Observations were undertaken at an accelerating voltage of 20 kV with a back scattered electron detector.

3. Results and Discussion

3.1 Physico-mechanical characterisation of long-term sodium sulphate deterioration

3.1.1 Visual inspection of AAS, HSR, and PC materials

Visual inspection revealed changes over time to the appearance of AAS, PC and HSR mortars in water and sodium sulphate solution (5 wt.% Na_2SO_4, 10 wt.% Na_2SO_4) under wet-dry cycles, see **Figure 2**. More specifically, it is found that the appearance of AAS-Water increases in surface roughness after 360 days with minimal spalling at the edges after 570 days. When AAS mortar (AAS-N5) was exposed to 5 wt.% Na_2SO_4, surface roughness was observed to increase prior to 360 days with efflorescence developed after 570 days of exposure. Increasing the sodium sulphate concentration to 10 wt.% (AAS-N10) increased efflorescence onset and area coverage with salt crystallisation obviously occurring after 90 days. After 450 days, visible cracking can be observed resulting in aggregate exposure. Study of Bakharev et al. [18] shows that the appearance of AAS immersing in Na_2SO_4 solutions remains intact even after 12 months, similar findings was given by Ye [37] and Ismail [19], so it could be found that the spalling of AAS mortars was accelerated by the sodium sulphate in wet-dry cycles. The feature spalling of AAS mortars (especially, AAS-N10) accords well with the characteristics of salt crystallization destroy [38], which could be explained by the development of crystallisation pressure and dissolution diffusion stress of sodium sulphate during the wet-dry cycles [39-42]. During the process of drying, as the solutions of sodium sulphate evaporated, the concentration of sodium sulphate would increase accordingly, which results in the growth of sodium sulphate crystals after achieving the saturation. Crystallisation pressure is formed, when sodium sulphate crystal encounters the wall of pores. It should be noted that the growth of sodium sulphate crystals in mortars not only generates crystallisation pressure, but also introduces the diffusion stress due to the fact that the crystals near flaw in mortars will re-dissolve and the sodium sulphate solute will diffuse to crystals growing within the flaw. As the crystals dissolve and their crystallisation pressure is released, the matrix near the flaw tends to contract (i.e., the matrix is no longer inflated by pressure from the crystals). However, the matrix farther from the flaw is still expanded by crystallisation pressure, so the defect keeps growing. This process will lead to growth of cracks as long as

sodium sulphate is diffusing into the flaw; the surface tensile strength of mortars will diminish as the flaws grow, and the body may collapse. Concurrently, horizontal and vertical cracking aligned with the sample edges appeared resembling a reaction front as commonly observed for other degradation phenomena [5], where the appearance of this cracking after wet-dry cycles also suggests the products of a drying-susceptible phase (i.e., silica gels). Subsequent sections will explain the long-term degradation mechanisms observed herein.

As expected, the appearance of PC mortar (PC-N5) was intact until 360 days and visible cracks appeared after 450 days with deleterious cracking observed at 570 days of exposure. And the appearance of HSR falling slightly severe after 570 days. From visual comparison, the AAS mortars reveal a higher resistance than PC and HSR mortars. Salt attack in PC mortars is well understood and can be explained by precipitation of calcium sulfate phases, which due to expansive volumes yield cracking tensile forces within the material's microstructure.

3.1.2 Compressive strength of AAS, HSR, and PC materials

When exposed to water, only a continuous increase of 0.5% in the compressive strength of AAS is observed after 270 days, see **Figure 3.** When exposed to 5 wt.% sodium sulphate solution, the compressive strength of the material increases in the initial 90 days of exposure followed by a 19.1% decrease at 270 days. In AAS-N10 samples a similar compressive strength gain as AAS-N5 samples is observed at 90 days of exposure, see **Figure 3-a**. The compressive strength of AAS-N10 sharply decreases by 47% after exposing sodium sulphate wet-dry cycles for 360 days. The initial increase in compressive strength of AAS mortars may be due to partial pore filling of sodium sulphate phases. Importantly, while current literature has agreed that sodium sulphate chemical attack is not detrimental in alkali-activated systems, and the compressive strength remain increase even after 25 months of immersing exposure [43]. In this study, the decrease of compressive strength of AAS mortars verifies that the degradation and loss of compressive strength occurs at much earlier time scales than previously studied (i.e., 90 days) [37]. It is believed that the compressive strength decrease is due to the crystallisation pressure [39] and the dissolution diffusion stress [40] of sodium sulphate under wet-dry cycles. Higher concentration of Na_2SO_4 produces bigger crystallisation pressure and the dissolution stress, resulting in sharply decrease of AAS-N10 at 360 days.

Interesting results could be found that, after the decease period of compressive strength AAS systems regain compressive strength (AAS-N5 reaching 80.7 MPa at 450 days and AAS-N10 reaching 53.2 MPa at 570 days). This phenomenon may be associated with the continuous reaction of unreacted precursor (exposed by crystallisation pressure and the diffusion stress of sodium sulphate), because Na_2SO_4 is one of the good activators for GGBFS [44]. This continuous reaction may introduce C(N)-A-S-H cementitious binders or aluminium incorporation of silica gels in AAS mortars, making the microstructure denser (see **Figure 6**) and improving the compressive strength. Lastly, from 450 days to 570 days, compressive strength of AAS-N5 decreases again. It is not hard to see that compressive strength development of AAS is a comprehensive result of physical/chemical action between Na_2SO_4 and unreacted precursor under wet-dry cycles.

For the comparison samples, the compressive strength of both PC and HSR samples increased firstly and decreased later (shown in **Figure 3-a**), which is consistent with the results of previous studies, e.g. Zhang [45], Jiang and Niu [46]. The compressive strength of PC-N5 decreased about 65% at 450 day, while most properties cannot be tested after this duration. For HSR-N5, the compressive strength decreased about 20% at 570 day. Considering that the compressive strength of AAS-N5 is almost the same as its initial value, it is clear that AAS mortars show greater resistance against sodium sulphate than PC and HSR mortars under wet-dry cycles.

3.1.3 Flexural strength of AAS, HSR, and PC materials

In this study, the development of flexural strength of AAS materials is not consistent with the development of compressive strength, which is not significant changed with age. The flexural strength of AAS mortars exposed to water increases slightly before 120 days, which could be attributed to the formation of silica gels due to

alkalinity loss and decalcification of C(N)-A-S-H gels [5]. While the flexural strength of AAS-N5 samples increases much higher than that of AAS-Water after one year of exposure with slight decreases after 450 days. It seems that sodium sulphate improved the flexural strength of AAS mortar under wetting-drying cycles. This is because, inner the AAS mortars, the exposed unreacted precursor due to crystallisation pressure [39] and dissolution diffusion stress can continue react in Na_2SO_4. And due to the loss of alkalinity and irreversible changes to the pore solution chemistry of the AAS materials, the reaction of the exposed precursor could induce subsequent silica-rich gel formation [47, 48]. It is important to note that the AAS material studied herein have a high silica content (Si:Al =2.1:1). The subsequent silica-rich gels could act as a role like short fibber at the micro-defects, thus the flexural strength of AAS mortars, in Na_2SO_4 solutions under wet-dry cycles, was improved. Encouraging findings could be seen in AAS-N10, where after a sharp decrease (could be attributed to the bigger crystallisation pressure and dissolution diffusion stress), the flexural strength increases faster after 270 days (see **Figure 4**). This could be explained by the fact that higher concentration of Na_2SO_4 leading to more sufficient reaction of the exposed precursor in AAS-N10. Clearly, the reaction of unreacted precursor is beneficial to mechanical property of AAS materials.

For PC and HSR samples, variations in flexural strength also follow the two features of general trend. The first is that the duration of flexural strength growth is around 50 days and the second is that the loss of strength is much more significant than that of AAS. The flexural strength of PC decreases to 2.01 MPa at 450 day while HSR performs better, as the reduction rate of flexural strength is slow. Despite of this, the loss of flexural strength of HSR is much higher than that of AAS-N5.

3.1.4 Mass change (M_c) of AAS, HSR, and PC materials

From **Figure 5-a**, a slight decrease is found for the mass of AAS-Water before 60 days and after this, no significant change can be identified. The initial loss of weight could be due to leaching of alkali ions in the samples [49, 50]. By comparison, the weight of AAS-N5 increases quickly before 120 days, clearly it is mainly the result of accumulation of sodium sulphate in pores. With the prolongation of age, the concentrated sodium sulphate in the pores gradually produces crystallisation pressure and dissolution diffusion stress, which leads to the surface efflorescence of the sample, and the mass of AAS-N5 shows a downward trend after 120 days. Interestingly, the weight of AAS-N5 shows a short period of increase during 270 to 450 days, because the mechanical properties of AAS-N5 were also strengthened during this period. This should be the result of the continuing reaction of exposed precursor and second pore-filling effects of sulphate phases. As the concentration of sodium sulphate increased to 10 wt.% (shown in **Figure 5-b**), the mass of AAS-N10 increases faster and the maximum value is higher than that of AAS-N5. Because the high concentrations of sodium sulphate can ingress fast in pores. In addition, the weight of AA-N10 drops fast after 90 days, which could be attributed to the severe peeling of surface layer as shown in **Figure 2**.

Comparing with PC-N5 and HSR-N5, the maximum mass of AAS-N5 is relatively low, which could be due to the small capillary porosity of AAS mortars (discussed later), in which a small amount of sodium sulphate crystals could be stored. Meanwhile, there are chemical reaction products in PC-N5 and HSR-N5 forming expansive erosion products [51]. In the long run, the weight of AAS is more stable and the ability to resist the damage of sodium sulfate is stronger.

3.1.5 Capillary porosity ($Ø_c$) of AAS, HSR, and PC materials

Important information could be obtained from the evolutions of capillary porosity of AAS mortars. From **Figure 6-a**, the capillary porosity of AAS-Water increases as the test duration also increases. It suggests that the capillary porosity of AAS mortar can be coarsen by wet-dry cycles, which could be attributed to volumetric instability of AAS [8, 52]. For AAS-N5, the capillary porosity drops significantly before 120 days due to accumulation of sodium sulphate in pores. However, after then the capillary porosity did not increase rapidly, although it was affected by both wet-dry cycles (enlarged the pores) and crystallisation pressure and diffusion stress. Especially, during the period from 270 to 450 days, where the capillary porosity becomes stable. And

during this period, the compressive/flexural strength increases. What's more, there were no typical sulphate erosion products, such as AFt and gypsum (see **Figure 8**) in AAS mortars, which maybe fill the pores [53]. These are strong indications of further reactions of exposed precursor that strengthen the matrix. As the concentration of sodium sulphate increased to 10 wt.%, a similar characterization could be found from 360 days to 570 days that the capillary porosity of AAS-N10 decreased slightly due to more sufficient reaction of the unreacted precursor. In other words, although the surface layer of AAS-N10 is severely peeled off, its core is still relatively dense. This is also a typical physical damage feature of AAS mortars under wet-dry cycles of sodium sulphate [38, 40].

Furthermore, the initial capillary porosity of AAS-N5 is not as high as PC and HSR mortars, which can explain its mass variation at the initial stage. At 570 day, the capillary porosity of the AAS mortar is much smaller than that of PC mortar, indicating that the overall structure of the AAS mortar is still relatively compact and the resistance to sodium sulphate attack of AAS mortar is stronger.

3.1.6 Water sorptivity (S) of AAS, HSR, and PC materials

Water sorptivity is one of the key factors that affect the transmission of mortar [54]. Changes in sorptivity of AAS, PC and HSR samples under the sodium sulphate attack are shown in **Figure 7**. As shown in **Figure 7-a**, no significant change in sorptivity of AAS-Water along the test duration can be identified. An increase in the sorptivity of AAS-N5 before 60 days could be seen, which is due to the accumulation of sodium sulphate in pores. To be precise, the dried sodium sulphate crystals (formed during the preparation of specimens) could regain chemical crystal water ($Na_2SO_4 + nH_2O \rightarrow Na_2SO_4 \cdot nH_2O$). The fast increase in sorptivity of AAS-N5 indicates that the migration of sodium sulphate in pores is fast [55], leading to high diffusion stress during the ion stage and further causes the mortar surface peeling off (as shown in **Figure 2**). As the concentration of sodium sulphate in the solution is increased to 10 wt.%, the sorptivity of AAS-N10 increases more rapidly, 3.8 times of the initial value after 180 days (shown in **Figure 7-b**). This caused higher diffusion stress of sodium sulphate, which resulted in more serious peeling of the surface layer of the specimen (as shown in **Figure 2**). Encouragingly, a sharp decrease in sorptivity of AAS-N10 is found after 180 days, this confirms the pore-dense action of continuing reaction products of unreacted GGBFS precursor.

Comparing to AAS, the sorptivity values of PC and HSR mortars are lower initially. This could be attributed to the high pore connectivity of AAS mortar [56] and more salt deposits [57] in the AAS samples. Numerous researchers, e.g. Collins and Sanjayan [58], Bernal et al. [54], Lawet al. [59], have reported the similar results. A rapid growth of sorptivity of PC-N5 after 270 days could be attributed to large cracks inside specimens and more sodium sulphate crystals in pores.

3.2 Physico-chemical micro-structural characterisation of long-term sodium sulphate deterioration

3.2.1 Mineralogy of AAS, HSR, and PC materials

The XRD results before and after 570 days' exposure to wet-dry cycles of sodium sulphate are given in **Figure 8**. It could be seen that before sulphate attacks the components of AAS mortars are quartz (SiO_2, 2θ=26.6°, 20.9° and 45.8°), calcite ($CaCO_3$, 2θ=27.1°, 32.8° and 50.1°) and C(N)-A-S-H gels (humps around 29.6° and 49.5°), while no portlandite is found [60]. The quartz is from the raw siliceous sand and the C(N)-A-S-H gels are the main reaction products. The calcite could be from carbonation during preparation of samples. After 570 days, the components of AAS mortars are similar to the components before attacking, and common deterioration calcium sulphate products (e.g., gypsum and AFt) are not observed during the wet-dry cycles likely due to the binder composition and lower calcium contents than PC materials [16]. These findings are consistent with results given by Khan et al. [61] and Dzunuzovic et al. [19]. Clearly, the severely peeling off of AAS mortars (as shown in **Figure 1**) is not caused by common deterioration or expansive products in AAS, e.g. AFt, during the wet-dry cycles of sodium sulphate. Focusing on the intensity of peaks around 29.6° and 49.5° (C(N)-A-S-H gels), interesting results could be found that intensity of AAS materials became higher after 570 days of wet-dry cycles in sodium sulphate, and the higher the concentration, the greater the increase. Higher

intensity of peaks usually means more products [62]. This is consistent with the further reaction of exposed unreacted precursor, that is, more unreacted slags were exposed due to crystallisation pressure and solution diffusion stress of high concentration sodium sulphate, and more sufficient continuing reaction of the unreacted precursor in high concentration sodium sulphate.

The initial components of PC and HSR mortars are similar, comprising of quartz, portlandite, calcite and C-S-H gels. After 570 days of wet-dry cycles, new phases-AFt (ettringite, 2θ=9.1°, 15.8° and 22.9°) and gypsum (2θ=11.6°, 20.7° and 29.1°), can be detected, which are consistent with results reported by Zhang et al. [45] and Schmidt et al. [63]. These expansive calcium sulphate products account for the serious damage of PC-N5.

3.2.2 BSE Imaging of AAS, HSR, and PC materials

The microstructure of samples under sodium sulphate attack was inspected using BSE images. The transport of sodium sulphate and its relevant chemical/physical reactions start from the surface, but the highest concentration is usually not at the surface layer. Because the pH value at surface layer is low due to leaching of alkali under wet-dry cycles, which results in sulphate phases unstable and re-dissolve into the solutions [64-66]. To highlight this feature, the BSE examinations were carried out at two location, 0.5mm from the exposure surface and 3mm from the exposure surface, the typical results of which are shown in **Figure 9**. As shown, both the 0.5 mm and 3 mm area of AAS-Water are dense after 570 days of wet-dry cycles by water. However, numerous cracks are found in 3 mm area of AAS-N5 mortars after 570 days of wet-dry cycles by sodium sulphate solution, while the 0.5 mm area is quite dense. This is mainly because the concentration of sodium sulphate in 0.5 mm area will arise during the dry cycles, and the sodium sulphate will diffuse into the solution during the wet cycles due to concentration gradient, and in 3 mm area the sodium sulphate will gradually accumulate [67]. What's more, cracking in 3mm area demonstrates a characteristic of map-style cracks (very unlike the cracks in PC and HSR mortars), suggesting the formation of cracks is mainly attributed to crystallisation pressure and diffusion stress of sodium sulphate in wet-dry cycles. As the concentration increased to 10 wt.%, AAS-N10 demonstrates large cracks in both 0.5 mm and 3 mm area due to high crystallisation pressure and diffusion stress. In addition, the content of unreacted slags in mortars could be estimated. Clearly, the content of unreacted slags in 3 mm area of AAS-N5 is lower than that of AAS-Water. This is consistent with the fact that unreacted slags inside AAS-N5 can continue to react in sodium sulphate solution under wetting-drying cycle. As expected, the content of unreacted slags in AAS-N10 is much lower.

3.2.3 FTIR Molecular Structure of AAS, HSR, and PC materials

Decalcification, formation of silica gels, and extended binder polymerization was verified via FTIR data, see **Figure 10.** After 570 days of cyclic sodium sulphate exposure, silica gels are formed as indicated by the formation of additional absorption peaks at 1080 cm^{-1} and 1086 cm^{-1} as well as appearance of the band at 778 cm^{-1} and bands at 976 cm^{-1} and 458 cm^{-1} (bending and stretching vibration [Si-O]) [68, 69]. The formation of these silica gels is likely due to wet-dry cycling causing a loss of alkalinity. This phenomenon would occur due to drying cycles decreasing solubility limits of aqueous species, such as monomeric silica, in the pore solution chemistry. These results may be particularly relevant in this study due to the high silicon content of AAS formulations studied (Si:Al= 2.1:1). Furthermore, contributions from extended slag reaction after 570 days is observed by a wavenumber shift from 974 cm^{-1} to 1014 cm^{-1} and 1016 cm^{-1} [70]. Contributions from continuous reaction of unreacted slag yield additional C(N)-A-S-H or another highly crosslinked cementitious binder.

The evolution of properties, such as compressive/flexural strength and porosity, of AAS mortars should be related with this formation of additional binder. In addition, absorption bands of gypsum and AFt are not detected in AAS mortars, which are consistent with the results of XRD. Lastly, the wavenumbers at 3449 cm^{-1} and 1635 cm^{-1} are related to [O-H] stretching of water [71], and the wave numbers at 875 cm^{-1} and 713 cm^{-1} correspond to out-of-plane bending modes of [CO_3] [72].

For PC and HSR mortars, the band at 3643 cm^{-1} is related to [O-H] stretching of portlandite [68], and the wave number at 1113 cm^{-1} corresponding to [SO_4] of gypsum and AFt. After 570 days, the band at 602 cm^{-1} related

to gypsum [19] appears in PC and HSR mortars. It is also noted that the intensity of transmittance corresponding to portlandite around 3643cm^{-1} becomes lower for PC-N5-570d and HSR-N5-570d, which could be attributed to the consumption of portlandite by sodium sulphate.

4. Conclusions

In this study, the degradation process of AAS mortars under wet-dry cycles was assessed by examining macroscopic and microscopic characteristics. On the basis of results obtained, the following conclusions could be made:

1) No deleterious calcium sulphate phases were observed to form, AAS mortars have little problem of sodium sulphate chemical attack, but physical damage under wet-dry cycles must be considered. Crystallisation pressure and diffusion stress of sodium sulphate may cause serious peeling off AAS mortar surface layer.

2) The continuous hydration behaviour of unreacted slag has a significant impact on the damage process of AAS mortars. The unreacted precursor slag, exposed due to crystallisation pressure and diffusion stress, can continue to react within sodium sulphate to form silicon-rich gels, which has repair function on micro-damages, making the failure process of AAS mortar shows certain performance recovery phenomenon.

3) After long-term durability studies, AAS samples performed better than PC and HSR samples exposed to wet-dry cyclic 5 wt.% sodium sulphate solutions. After 570 days, the compressive strength of AAS mortar decreased slightly, while the compressive strength of PC mortar was reduced by more than 65%, and the compressive strength loss of HSR mortar was about 20%. AAS materials maintained higher compressive strengths, flexural strengths, and with lower capillary porosity.

The failure process of AAS mortars under the wet-dry cycles of sodium solution is complicated and it is not able to clarify this mechanism in one study. More fundamental researches on the stability of reaction products, crystallisation process and conditions in this process, are needed.

Acknowledgements

The authors acknowledge the following institutions for providing facilities and the financial support: National Natural Science Foundation of China (NO. 51878102 and 51778089), Guangxi Innovation Drive Major Project (2018AA23004), Open funds from Shenzhen University, Chongqing Foundation Research Program. In addition, supports provided from University of Leeds during analysis of data and preparation of this paper are also highly appreciated.

References

[1] S. A. Miller, V. M. John, S. A. Pacca, et al., Carbon dioxide reduction potential in the global cement industry by 2050, Cement and Concrete Research. 114 (2018) 115-124.

[2] M. B. Haha, G. Le Saout, F. Winnefeld, et al., Influence of activator type on hydration kinetics, hydrate assemblage and microstructural development of alkali activated blast-furnace slags, Cement and Concrete Research. 41 (2011) 301-310.

[3] F. Pacheco-Torgal, J. Castro-Gomes and S. Jalali, Alkali-activated binders: A review-Part 1. Historical background, terminology, reaction mechanisms and hydration products, Construction and Building Materials. 22 (2008) 1305-1314.

[4] F. Pacheco-Torgal, J. Castro-Gomes and S. Jalali, Alkali-activated binders: A review. Part 2. About materials and binders manufacture, Construction and Building Materials. 22 (2008) 1315-1322.

[5] J. P. Gevaudan, A. Caicedo-Ramirez, M. T. Hernandez, et al., Copper and cobalt improve the acid resistance of alkali-activated cements, Cement and Concrete Research. 115 (2019) 327-338.

[6] M. C. G. Juenger, F. Winnefeld, J. L. Provis, et al., Advances in alternative cementitious binders, Cement and Concrete Research. 41 (2011) 1232-1243.

[7] E. Gartner, Industrially interesting approaches to “low-CO2” cements, Cement and Concrete Research. 34 (2004) 1489-1498.

[8] H. Ye, C. Christopher, F. Rajabipour et al., Understanding the drying shrinkage performance of alkali-activated slag mortars, Cement and Concrete Composites. 76 (2017) 13-24.

[9] H. Ye and A. Radlińska, Shrinkage mitigation strategies in alkali-activated slag, Cement and Concrete Research. 101 (2017) 131-143.

[10] A. Ferna´ndez-Jime´nez and F. Puertas, The alkali-silica reaction in alkali-activated granulated slag mortars with reactive aggregate, Cement and Concrete Research. 32 (2002) 1019-1024.

[11] R. Tänzer, Y. Jin and D. Stephan, Effect of the inherent alkalis of alkali activated slag on the risk of alkali silica reaction, Cement and Concrete Research. 98 (2017) 82-90.

[12] W. Aperador, R. M. de Gutiérrez and D. M. Bastidas, Steel corrosion behaviour in carbonated alkali-activated slag concrete, Corrosion Science. 51 (2009) 2027-2033.

[13] M. Komljenović, Z. Baščarević, N. Marjanović, et al., External sulfate attack on alkali-activated slag, Construction and Building Materials. 49 (2013) 31-39.

[14] N. Džunuzović, M. Komljenović, V. Nikolić, et al., External sulfate attack on alkali-activated fly ash-blast furnace slag composite, Construction and Building Materials. 157 (2017) 737-747.

[15] J. Li, W. Zhang, K. Garbev, et al., Influences of cross-linking and Al incorporation on the intrinsic mechanical properties of tobermorite, Cement and Concrete Research. 136 (2020) 106170.

[16] R. J. Myers, S. A. Bernal, J. D. Gehman, et al., The role of Al in cross-linking of alkali-activated slag cements, Journal of the American Ceramic Society. 98 (2015) 996-1004.

[17] E. Douglas, A. Bilodeau and V. M. Malhotra, Properties and durability of alkali-activated slag concrete, ACI Materials Journal. 89 (1992) 509-516.

[18] T. Bakharev, J. G. Sanjayan and Y. B. Cheng, Sulfate attack on alkali-activated slag concrete, Cement and Concrete Research. 32 (2002) 211-216.

[19] I. Ismail, S. A. Bernal, J. L. Provis, et al., Microstructural changes in alkali activated fly ash/slag geopolymers with sulfate exposure, Materials and Structures. 46 (2013) 361-373.

[20] E. Ganjian and H. S. Pouya, The effect of Persian Gulf tidal zone exposure on durability of mixes containing silica fume and blast furnace slag, Construction and Building Materials. 23 (2009) 644-652.

[21] E. Gruyaert, P. Van den Heede, M. Maes, et al., Investigation of the influence of blast-furnace slag on the resistance of concrete against organic acid or sulphate attack by means of accelerated degradation tests, Cement and Concrete Research. 42 (2012) 173-185.

[22] Q. Li, K. Yang, C. H. Yang, An alternative admixture to reduce sorptivity of alkali-activated slag cement by optimising pore structure and introducing hydrophobic film, Cement and Concrete Composites. 95 (2019) 183-192.

[23] K. Yang, C. H. Yang, B. Magee, et al., Establishment of a preconditioning regime for air permeability and sorptivity of alkali-activated slag concrete, Cement and Concrete Composites. 73 (2016) 19-28.

[24] F. Puertas, A. Fernández-Jiménez and M. T. Blanco-Varela, Pore solution in alkali-activated slag cement pastes. Relation to the composition and structure of calcium silicate hydrate, Cement and Concrete Research. 34 (2004) 139-148.

[25] M. Babaee and A. Castel, Water vapor sorption isotherms, pore structure, and moisture transport characteristics of alkali-activated and Portland cement-based binders, Cement and Concrete Research. 113 (2018) 99-120.

[26] Q. Li, Y. Yang, K. Yang, et al., The role of calcium stearate on regulating activation to form stable, uniform and flawless reaction products in alkali-activated slag cement, Cement and Concrete Composites. 103 (2019) 242-251.
[27] Chinise GB-175, Common Portland cement, Standardization administration of the reople's republic of China. Beijing (2007) 6 pages.
[28] E.F. Irassar, M. Gonzalez and V. Rahhal, Sulphate resistance of type V cements with limestone filler and natural pozzolana, Cement and Concrete Composites. 22 (2000) 361-368.
[29] D. Mostofinejad, F. Nosouhian and H. Nazari-Monfared, Influence of magnesium sulphate concentration on durability of concrete containing micro-silica, slag and limestone powder using durability index, Construction and Building Materials. 117 (2016) 107-120.
[30] Z. Makhloufi, S. Aggoun, B. Benabed, et al., Effect of magnesium sulfate on the durability of limestone mortars based on quaternary blended cements, Cement & Concrete Composites. 65 (2016) 186-199.
[31] Chinise GT-17671, Method of testing cements-determination of strength, The state bureau of quality and technical supervision. Beijing (1999) 9 pages.
[32] ASTM C642, Standard test method for density, absorption, and voids in hardened concrete1, ASTM Standard. (2013).
[33] ASTM C1585, Standard test method for measurement of aate of absorption of water by hydraulic cement concretes, ASTM Standard. (2013)
[34] RILEM TC 116-PCD. Permeability of concrete as a criterion of its durability, Mater Struct V. 32 (1999) 174-179.
[35] BS-EN:13057, Products and systems for the protection and repair of concrete structures-test methods: determination of resistance of capillary absorption, BSI. London (2002) 1-16.
[36] British Standards Institution (BSI), Testing concrete-method for determination of water absorption, BS 1881-122, London. (2011).
[37] H. Ye, Z. Chen and L. Huang, Mechanism of sulfate attack on alkali-activated slag: The role of activator composition, Cement and Concrete Research. 125 (2019) 105868.
[38] H. Haynes, R. O'Neill, M. Neff, et al., Salt Weathering distress on concrete exposed to sodium sulfate environment, ACI Materials Journal. 105 (2008) 34-43.
[39] G. W. Scherer, Stress from crystallization of salt, Cement and Concrete Research. 34 (2004) 1613-1624.
[40] N. Thaulow and S. Sahu, Mechanism of concrete deterioration due to salt crystallization, Materials Characterization. 53 (2004) 123-127.
[41] G. W. Scherer, Factors affecting crystallization pressure. International RILEM TC 186-ISA workshop on internal sulfate attack and delayed ettringite formation. 4-6 September (2002)
[42] [20] G. W.Scherter, Crystallization in pores. Cement and Concrete Research. 29 (1999) 1348-1358.
[43] H. Kukko, R. Mannonen, Chemical and mechanical properties of alikali-activated blast furnace slag (F-concrete), Nordic Concrete Research. 1 (1982) 1-16.
[44] A. M. Rashad, Y. Bai, P. A. M. Basheer, et al., Chemical and mechanical stability of sodium sulfate activated slag after exposure to elevated temperature, Cement and Concrete Research. 42 (2012) 333-343.
[45] Z. Zhang, X. Jin and W. Luo, Long-term behaviors of concrete under low-concentration sulfate attack subjected to natural variation of environmental climate conditions, Cement and Concrete Research. 116 (2019) 217-230.
[46] L. Jiang and D. Niu, Study of deterioration of concrete exposed to different types of sulfate solutions under drying-wetting cycles, Construction and Building Materials. 117 (2016) 88-98.
[47] J. Yang, D. Li and Y. Fang, Effect of synthetic CaO-Al2O_3-SiO_2-H_2O on the early-stage performance of alkali-activated slag, Construction and Building Materials. 167 (2018) 65-72.
[48] M. Zhang, M. Jiang and J. Chen, Variation of flexural strength of cement mortar attacked by sulfate ions, Engineering Fracture Mechanics. 75 (2008) 4948-4957.
[49] M. H. T. Hubler, J. J. Thomas and H. M. Jennings, Influence of nucleation seeding on the hydration kinetics and compressive strength of alkali activated slag paste, Cement and Concrete Research. 41 (2011) 842-846.
[50] M. Hubler, H. Jennings and J.Thomas, Influence of nucleation seeding on the compressive strength of ordinary portland cement and alkali-activated blast-furnace slag, Journal of School Psychology. 17 (2011) 172-180.
[51] S. U. Al-Dulaijan, M. Maslehuddin, M. M. Al-Zahrani, et al., Sulfate resistance of plain and blended cements exposed to varying concentrations of sodium sulfate, Cement and Concrete Composites. 25 (2003) 429-437.
[52] X. Zhu, D. Tang, K. Yang, et al., Effect of $Ca(OH)_2$ on shrinkage characteristics and microstructures of alkali-activated slag concrete, Construction and Building Materials. 175 (2018) 467-482.
[53] A. Neville, The confused world of sulfate attack on concrete, Cement and Concrete Research. 34 (2004) 1275-1296.
[54] S. A. Bernal, R. Mejía de Gutiérrez, A. L. Pedraza, et al., Effect of binder content on the performance of alkali-activated slag concretes, Cement and Concrete Research. 41 (2011) 1-8.

[55] L. Hanžič and R. Ilić, Relationship between liquid sorptivity and capillarity in concrete, Cement and Concrete Research. 33 (2003) 1385-1388.
[56] X. Zhu, Z. Zhang, K. Yang, et al., Characterisation of pore structure development of alkali-activated slag cement during early hydration using electrical responses, Cement and Concrete Composites. 89 (2018) 139-149.
[57] A. R. Brough and A. Atkinson, Sodium silicate-based, alkali-activated slag mortars Part I. Strength, hydration and microstructure, Cement and Concrete Research. 32 (2002) 865-879.
[58] F. Collins and J. Sanjayan, Unsaturated capillary flow within alkali activated slag concrete, Journal of Materials in Civil Engineering. 20 (2008) 565-570.
[59] D. W. Law, A. A. Adam, T. K. Molyneaux, et al., Durability assessment of alkali activated slag (AAS) concrete, Materials and Structures. 45 (2012) 1425-1437.
[60] X. H. Zhu, X. J. Kang, K. Yang, et al., Effect of graphene oxide on the mechanical properties and the formation of layered double hydroxides (LDHs) in alkali-activated slag cement, Construction and Building Materials. 132 (2017) 290-295.
[61] H. A. Khan, M. S. H. Khan, A. Castel, et al., Deterioration of alkali-activated mortars exposed to natural aggressive sewer environment, Construction and Building Materials. 186 (2018) 577-597.
[62] K. L. Scrivener, T. Füllmann, E. Gallucci, et al., Quantitative study of Portland cement hydration by X-ray diffraction/Rietveld analysis and independent methods, Cement and Concrete Research. 34 (2004) 1541-1547.
[63] T. Schmidt, B. Lothenbach, M. Romer, et al., Physical and microstructural aspects of sulfate attack on ordinary and limestone blended Portland cements, Cement and Concrete Research. 39 (2009) 1111-1121.
[64] F. Weritz, A. Taffe, D. Schaurich, et al., Detailed depth profiles of sulfate ingress into concrete measured with laser induced breakdown spectroscopy. Construction and Building Materials. 23 (2009) 275-283.
[65] [17] R. D. Gao, Q. B. Li and S. B. Zhao, Concrete deterioration mechanisms under combined sulfate atack and flexural loading, Journal of Materials in Civil Engineering. 25 (2013) 39-44.
[66] [18] J. Stroh, M. C. Schlegel, E. F. Irassar, et al., Applying high resolution SyXRD analysis on sulfate attacked concrete field samples, Cement and Concrete Research. 66 (2014) 19-26.
[67] B. Lothenbach, B. Bary, P. Le Bescop, et al., Sulfate ingress in Portland cement, Cement and Concrete Research. 40 (2010) 1211-1225.
[68] I. García Lodeiro, D. E. Macphee, A. Palomo, et al., Effect of alkalis on fresh C-S-H gels. FTIR analysis, Cement and Concrete Research. 39 (2009) 147-153.
[69] N. Li, N. Farzadnia and C. Shi, Microstructural changes in alkali-activated slag mortars induced by accelerated carbonation, Cement and Concrete Research. 100 (2017) 214-226.
[70] S. A. Bernal, J. L. Provis, V. Rose, et al., Evolution of binder structure in sodium silicate-activated slag-metakaolin blends, Cement and Concrete Composites. 33 (2011) 46-54.
[71] N. Mobasher, S. A. Bernal and J. L. Provis, Structural evolution of an alkali sulfate activated slag cement, Journal of Nuclear Materials. 468 (2016) 97-104.
[72] Z. Shi, C. Shi, S. Wan, et al., Effect of alkali dosage and silicate modulus on carbonation of alkaliactivated slag mortars, Cement and Concrete Research. 113 (2018) 55-64.

Table 1 The chemical composition of raw materials (wt.%)

Binder	SiO_2	Al_2O_3	Fe_2O_3	MgO	CaO	Na_2O	K_2O	SO_3	LOI	Si:Al	Ca:Al
GGBFS	34.52	13.65	1.36	9.15	39.57	0.35	0.47	0.26	0.57	2.1:1	2.6:1
PC	22.54	5.47	2.64	2.74	62.1	0.61	0.18	0.57	3.14	3.5:1	95.6:1
HSR	28.44	0.62	1.04	2.09	65.1	0.21	0.18	1.57	0.74	38.9:1	10.3:1

Table 2 Mixture proportions for all AAS, PC, HSR cement samples utilized in this study

Groups	Parameters				
	Water/Binder	Binder/Sand	NaOH (g)	Water glass (g)	Binder (g)
AAS	0.45	1:3	9.5	96	450
PC	0.45	1:3	--	--	450
HSR	0.45	1:3	--	--	450

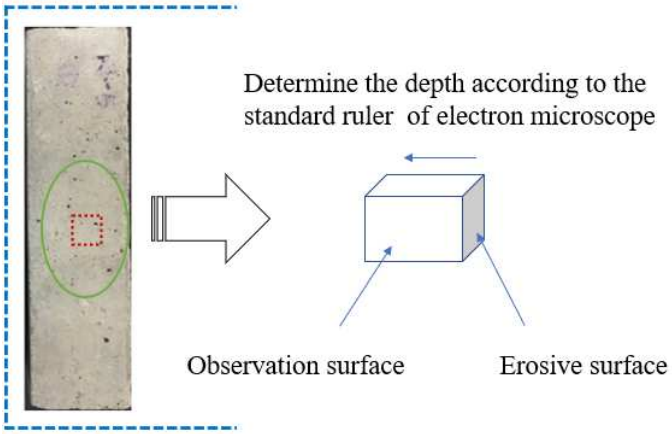

Figure 1 Schematic diagram of sample preparation for BSE

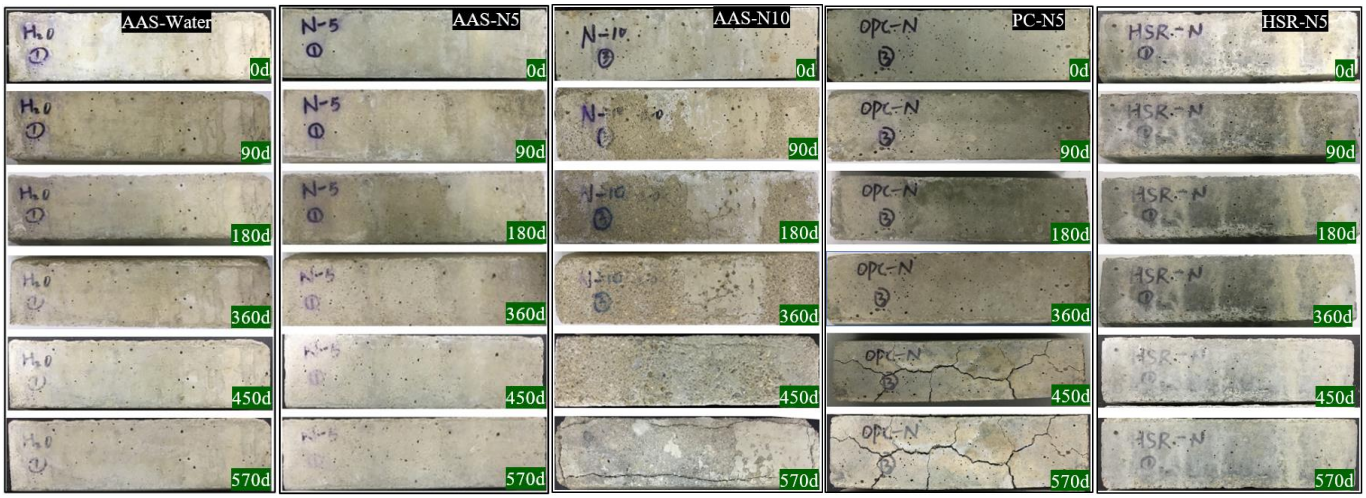

Figure 2 Appearance of the PC, HSR and AAS specimens under wet-dry cycles of sodium sulphate

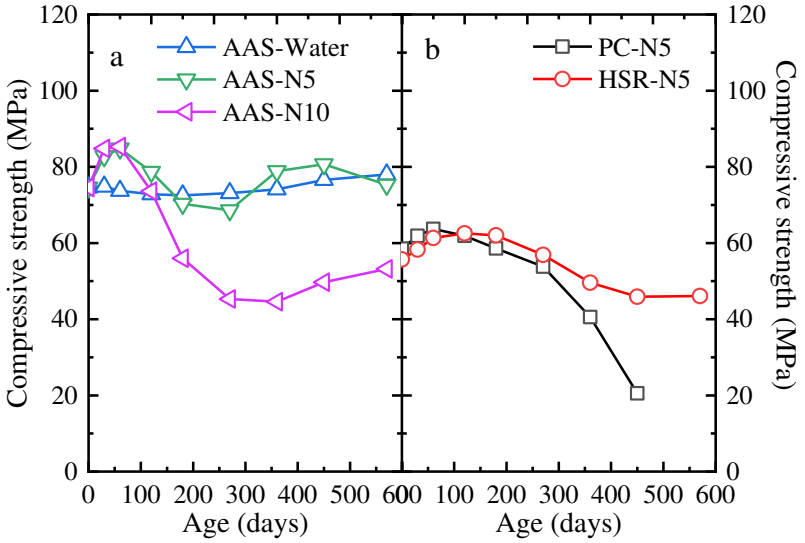

Figure 3 Compressive strength of AAS, PC and HSR samples under wet-dry cycles of sodium sulphate

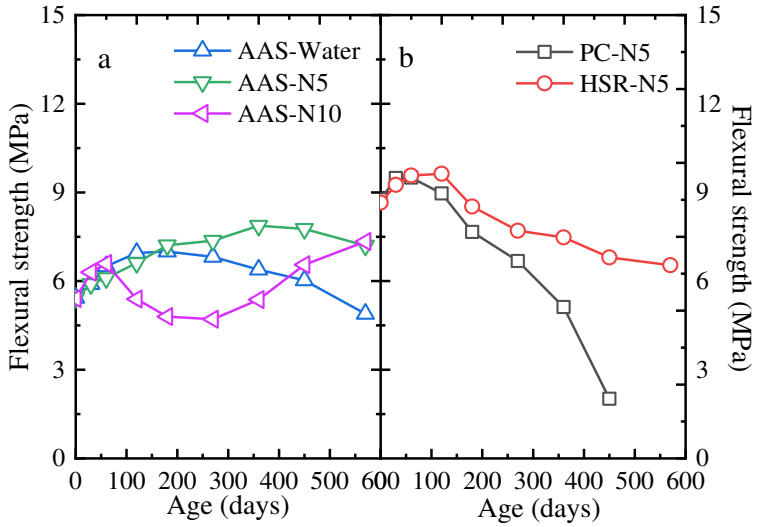

Figure 4 Flexural strength of AAS, PC and HSR under wet-dry cycles of sodium sulphate

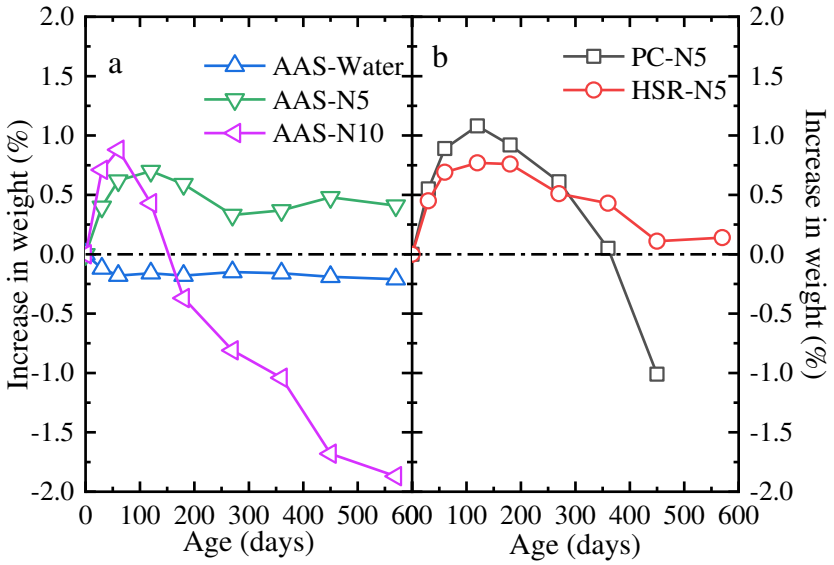

Figure 5 Increase in weight of AAS, PC and HSR under wet-dry cycles of sodium sulphate

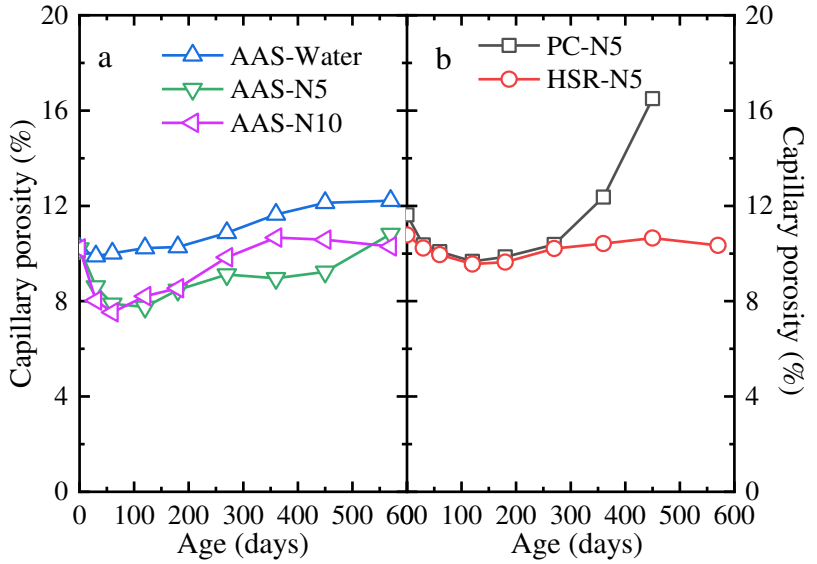

Figure 6 Capillary porosity of AAS, PC and HSR under wet-dry cycles of sodium sulphate

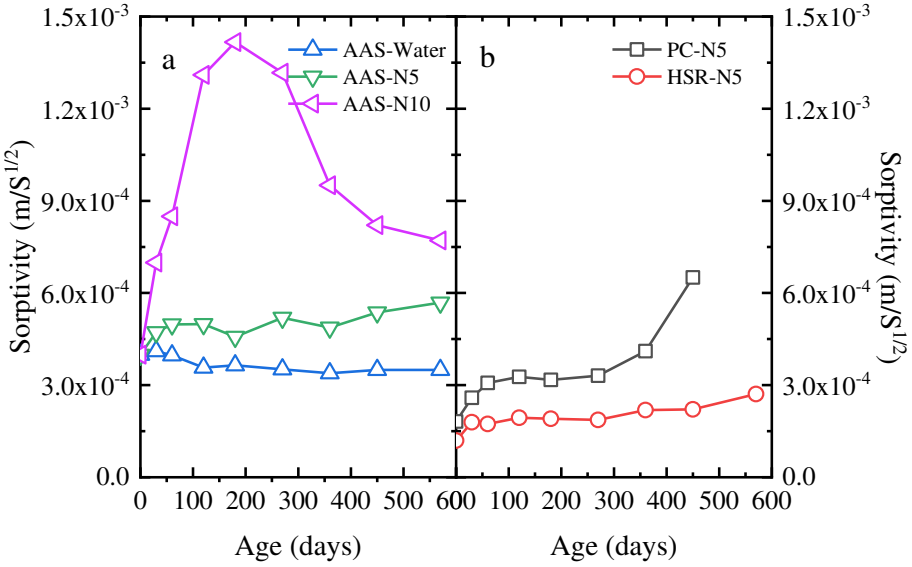

Figure 7 Sorptivity of AAS, PC and HSR under wet-dry cycles of sodium sulphate

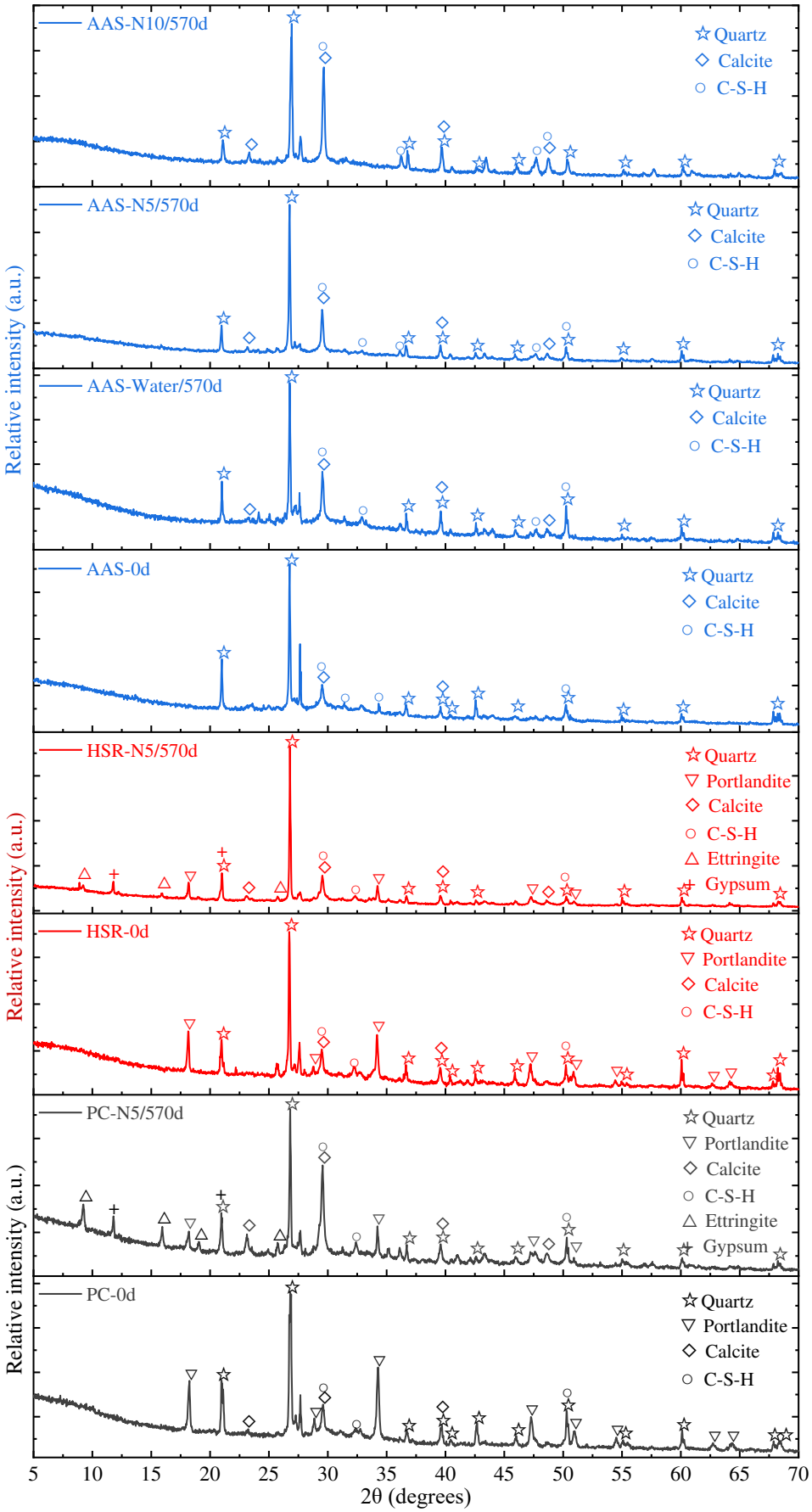

Figure 8 XRD patterns of AAS, PC and HSR samples at the attacking age of 0 day and 570 days

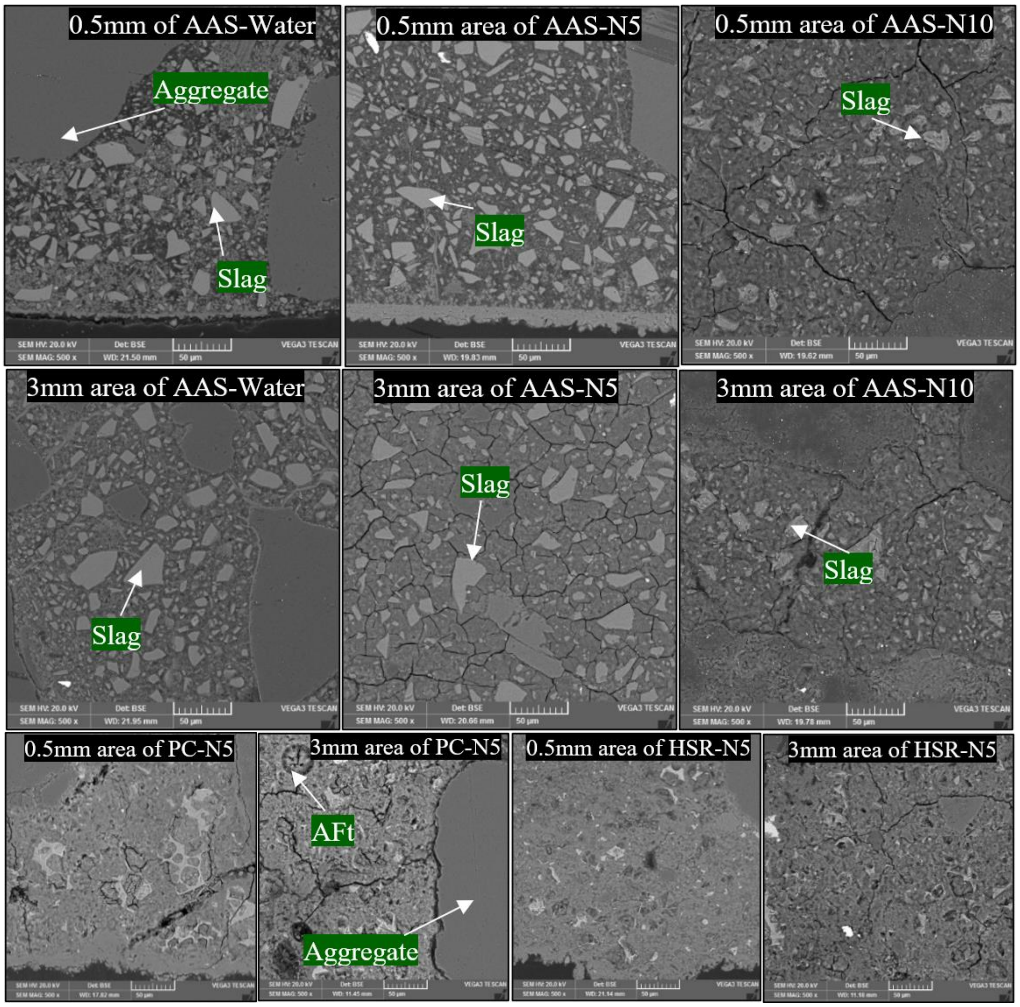

Figure9 BSE images of AAS, PC and HSC mortar samples at 570 days

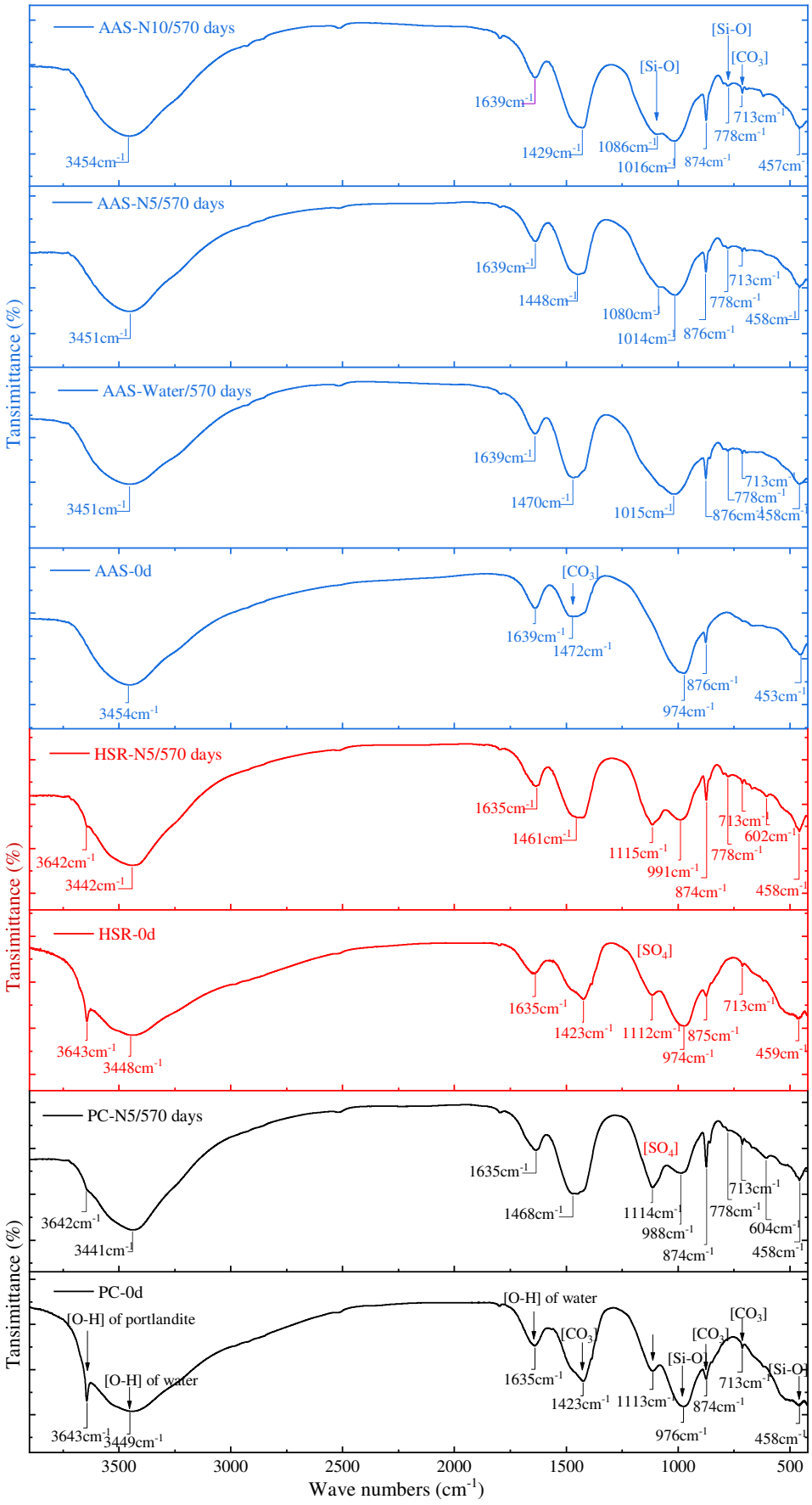

Figure 10 FTIR patterns of AAS, PC and HSR samples at the attacking age of 0 day and 570 days